Materials Science in Semiconductor Processing 15 (2012) 492–498

Contents lists available at SciVerse ScienceDirect

Materials Science in Semiconductor Processing

journal homepage: www.elsevier.com/locate/mssp

Pulsed laser deposition and characterization of $La_{1-x}Sr_xMnO_3$

S. Calderón V [a,c,*], L. Escobar-Alarcón [b], Enrique Camps [b], S. Rodil [c], I. Betancourt [c], J.J. Olaya [a]

[a] Universidad Nacional de Colombia, Bogotá, Colombia
[b] Instituto Nacional de Investigaciones Nucleares (ININ), México D.F., Mexico
[c] Instituto de Investigaciones en Materiales, Universidad Nacional Autónoma de México, México D.F., Mexico

ARTICLE INFO

Available online 29 March 2012

Keywords:
Ellipsometry
Manganites
Magnetic oxides

ABSTRACT

$La_{1-x}Sr_xMnO_3$ manganite films with $x=0.15$, 0.33 and 0.4 were deposited onto silicon substrates by pulsed laser deposition in an 80/20 Ar/O_2 atmosphere at room temperature. After being deposited, the films were annealed at 900 °C in air in order to obtain the desired crystalline phase. Structural characterizations using X-Ray diffraction showed polycrystalline compounds having the predominant peaks corresponding to the perovskite structure. Morphological studies carried out by scanning electron microscopy revealed a very rough surface and led to deducing the nature of the growth process. Spectral ellipsometry was performed between 1.5 and 5 eV range at room temperature, showing electronic transitions near to 2.2 and 4.7 eV in a range of thicknesses between 94 and 107 nm.

1. Introduction

Lanthanum-based manganites have been widely studied because of their outstanding colossal magnetoresistance (CMR) effect. They were first described in 1950 as being ferromagnetic materials having a magnetic transition usually accompanied by an electrical change, giving these materials the possibility of varying their electric conductivity by some orders of magnitude [1]. The general formula for these types of manganites is $A_{1-x}B_xMnO_3$, where A is a rare earth atom and B is a divalent ion such as Sr, Ca or Ba [2]. The magnetic, transport and magnetoresistance properties of these materials strongly depend on the quantity of the dopant B atom. For instance, changing the percentage of the Sr on the $LaSrMnO_3$ from 10% to 20%, significantly alters the magnetic phase of the compound [3]. Moreover, a phase diagram reported in [3] shows that partial substitutions of La by Sr inducing an extremely diverse behavior related to the magnetic phases and electrical response of this compound due to the spontaneous order of Mn^{+3}/Mn^{+4}. Additionally, some studies on La-based thin films have shown that such properties not only depend on the dopant content but also on the thickness of the coating and the substrate used [4,5]. For instance, Terzzoli et al. [6] reported that the transition temperature of $La_{0.67}Sr_{0.33}MnO_3$ films changed between 175 K and $T>325$ K depending on the substrate used.

Despite of the enormous advances achieved by several researches worldwide in regard to the properties of manganites' thin films, few reports have been published in the optical spectroscopy field aimed at describing the electronic transitions of these types of materials. Moritomo [7] has studied the dependency of the absorption coefficient as a function of temperature, showing a proportional relation between the temperature independent part of this coefficient and $1-M/M_s$ (where M is the films' magnetization and M_s is the film saturation magnetization). Complementarily, Kaplan and Mahanti [8] have also reported the presence of two absorption peaks: the 1.5 eV peak which is attributed to an interatomic transition and the 4.5 eV peak considered as being charge transference from the O 2p level to the Mn 3d level, confirming the double exchange behavior of the manganites.

* Corresponding author at: Universidad Nacional de Colombia, Bogotá, Colombia.
E-mail address: secave44@gmail.com (S. Calderón V).

1369-8001/$ - see front matter © 2012 Elsevier Ltd. All rights reserved.
http://dx.doi.org/10.1016/j.mssp.2012.03.009

In this paper, a systematic study on the structural and morphological properties of $LaSrMnO_3$ manganites is reported, as well as the film optical properties obtained by spectroscopy ellipsometry.

2. Experimental details

$La_{1-x}Sr_xMnO_3$ films with $x=0.15$, 0.33 and 0.4 were grown on silicon (1 0 0) substrates at room temperature by pulsed laser deposition (PLD) using a 1064 nm Nd:YAG laser with 5 ns pulse duration and a pulse frequency of 10 Hz. Beam's energy was measured and maintained at around 290 mJ, with 2.07 mm spot size. Total energy density deposited on the target (fluence) was fixed at 8.5 J/cm^2. The base pressure in the chamber was about 8×10^{-6} Torr and during the depositions the chamber was backfilled up to 7.5×10^{-2} Torr with an 80/20 Ar/O_2 mixture. Substrates were placed 5 cm from the targets to obtain homogenous films. Three depositing times were used in order to achieve different thicknesses. After deposition, films were air annealed at 900 °C for 1 h. Three targets, prepared by solid state reaction, were used in order to achieve the desired compositions ($x=0.15$, $x=0.33$, and $x=0.4$). Targets were annealed within a range of 950–1300 °C to evaluate the dependency of the temperature on the $LaSrMnO_3$ synthesis. X-ray diffraction (XRD) measurements were performed using a D8 Bruker diffractometers with Cu-Kα radiation ($\lambda=1.5406$ Å) in order to obtain the structural characteristics of the targets, while grazing incidence X-ray diffraction (GIXRD) was performed by means of a Siemens D-5000 with Cu-Kα radiation ($\lambda=1.5406$ Å) at 0.02° steps to determine the crystalline phase of the films. Composition and morphology were analyzed using scanning electron microscopy (SEM) and energy dispersive spectroscopy (EDS) using a SEM Cambridge-Leica model Stereo Scan 440. Optical properties were studied by means of a Horiba Jobin Yvon spectroscopic ellipsometer within a range of 1.5–5 eV with 0.05 eV interval step, using three incidence angles (60°, 65° and 70°). A classic Drude–Lorentz model was used to fit the data, considering the substrate, film and roughness layer. Additionally, magnetic properties such as magnetoresistance and magnetic hysteresis curves have been reported elsewhere [9], reveling materials with colossal magnetoresistance properties.

3. Results

3.1. Structural and morphological characterization

Fig. 1(a) shows an example of the evolution of $LaSrMnO_3$ targets' crystallization depending on the annealing temperature. It is clear that at 950 °C the synthesis of the compound was not completed, presenting a mixture between $LaSrMnO_3$ and a precursor phase (La_2O_3). Subsequently, at 1200 °C, XRD confirmed the absence of precursor's phases. However, it was necessary to increase the temperature since the cohesion between the particles was not adequate to maintain integrity of the targets during the PLD process (see Fig. 2).

Fig. 1(b) presents the X-ray diffraction patterns for the films deposited using the three different target compositions. It may be seen that the polycrystalline phases for each coating is either without any preferential orientation or secondary phases. The patterns were consistent with the pattern from database ICDD-PDF 47-0444 (10% of strontium), 50-0308 (33% of strontium) and 51-0118 (40% of strontium). It should be stressed that annealing the samples after the deposition was determinant in obtaining the crystalline phase in the films since they were not crystalline as deposited. Furthermore, annealing duration was not significant since variable heat treatments during 10, 20, 30, 40, 50 and 60 min showed similar results in the XRD patterns.

The Scherrer formula was used to calculate the grain size for each coating, obtaining the smallest grain size for the 40% of strontium concentration in the films. Table 1 presents the grain sizes for all the films deposited. Though the

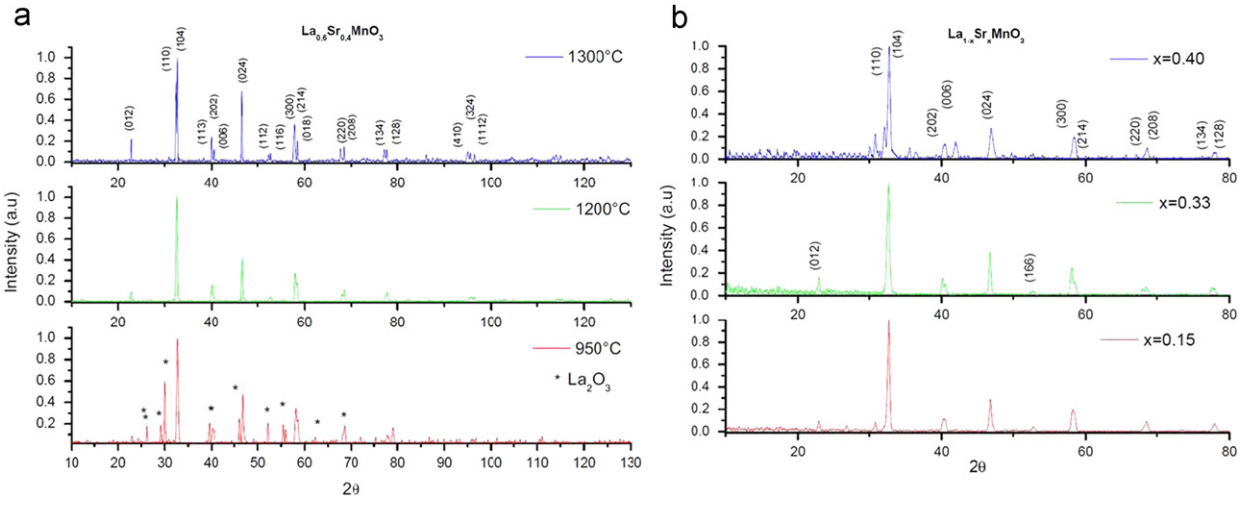

Fig. 1. (a) X-ray diffraction (XRD) evolution of $La_{0.65}Sr_{0.4}MnO_3$ target at different annealing temperatures and (b) XRD of $La_{1-x}Sr_xMnO_3$ ($x=0.15$, $x=0.33$ and $x=0.40$) films on Si substrate.

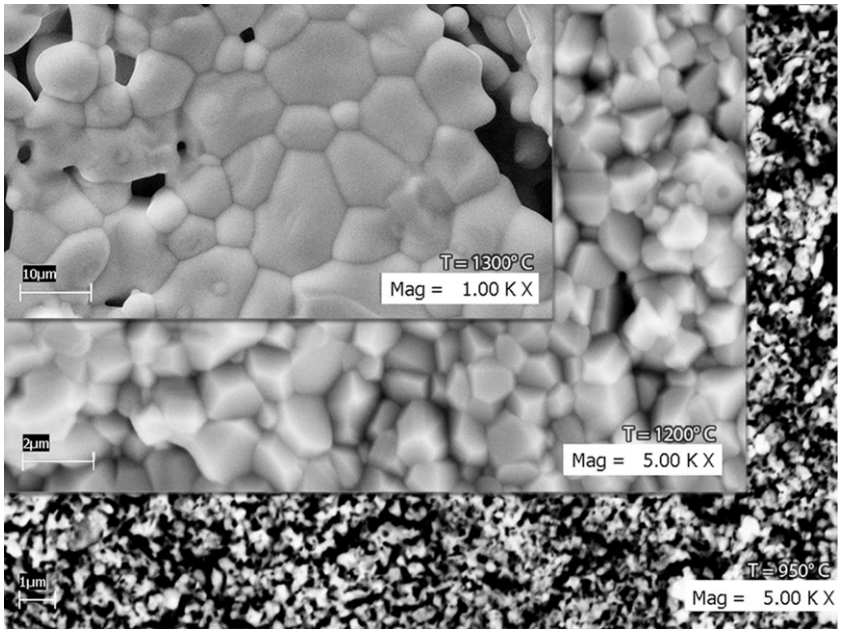

Fig. 2. Scanning electron microscopy image for $La_{0.85}Sr_{0.15}MnO_3$ target at 950 °C (botton), 1200 °C (middle) and 1300 °C (top).

Table 1
Grain size for $La_{1-x}Sr_xMnO_3$ with $x=0.15$, 0.33 and 0.4 calculated by Scherrer formula at different planes.

%Sr	Grain size (nm) plane (1 0 4)	Grain size (nm) plane (2 0 2)	Grain size (nm) plane (0 2 4)
15	22.9	26.9	23.1
33	23.4	27.9	28.5
40	22.3	24.6	17.1

grain size is around 25 nm, the films showed a very rough surface, with large agglomerates of the material of several sizes, attaining values of up to 1 μm of diameter dispersed on the entire surface. This is mainly a consequence of the high energy used during the laser ablation process. On this basis, the thinnest films were selected to perform the optical measurements, since these films also presented lower roughness values and therefore the scattering of the incident light was minimized. Fig. 3 illustrates the surface morphology for the 500 nm film, as can be evidenced by the cross-section image shown in the inset. On the other hand Fig. 4 displays the cross-section image from a 100 nm sample, where it can be observed that the circular features on the surface are smaller. Similar surface morphologies were observed for the other compositions, suggesting that it is mainly a consequence of the preparation technique. This agglomeration and clustering typically occurred when pulsed laser deposition at high energies is used.

3.2. Optical spectroscopy

For the ellipsometry analysis, spectra are reported as *Is* and *Ic*, which are the experimental measurements in a phase modulated ellipsometer [10]. A classic Drude–Lorentz model was used to parameterize the optical functions of the $LaSrMnO_3$ compound (Eq. (1)). A two layer structure (plus the substrate) was considered in the model in order to take into account the surface roughness. The top or roughness layer was modeled using a Bruggeman effective medium approximation composed of 50% $LaSrMnO_3$ and 50% voids. The $LaSrMnO_3$ layer was modeled using the Drude–Lorentz dielectric model [3].

$$\varepsilon = \varepsilon_\infty + \frac{(\varepsilon_s+\varepsilon_\infty)w_t^2}{w_t^2+w^2+i\Gamma_o w} + \sum_{j=1}^{2}\frac{f_j w_{oj}^2}{w_{oj}^2-w^2+i\gamma_j w} \quad (1)$$

where w is the light energy (eV), e_∞ is the dielectric constant for high energies, e_s is the static dielectric constant, w_t and Γ_o are the transition energy and damping constant of the main absorption process (band-edge) respectively, while f is the oscillator strength, w_o is the transition energy and t is the damping constant of the secondary absorption processes.

The actual determination of the model parameters was carried out using the Levenberg–Marquardt algorithm to minimize the difference between the measured and fitted spectra. Fig. 5 shows the fitting to the ellipsometry data from 1.5 to 5 eV using the structural model already described. The figures of merit (χ^2) was 1.76, 4.99, 5.21 for 40%, 33% and 15% Sr sample, respectively, indicating the validity of the parameterization for the dielectric function and the structural models. Moreover, the calculated thickness using this model resulted in a very accurate value compared to the thickness measured by SEM, obtaining values around 98.6 ± 7.3 nm (see Table 2).

The evolution of the real and imaginary component of the dielectric function depending on the Sr concentration is shown in Fig. 6.

The absorption coefficient for each composition is shown in Fig. 7, where it can be observed that for the

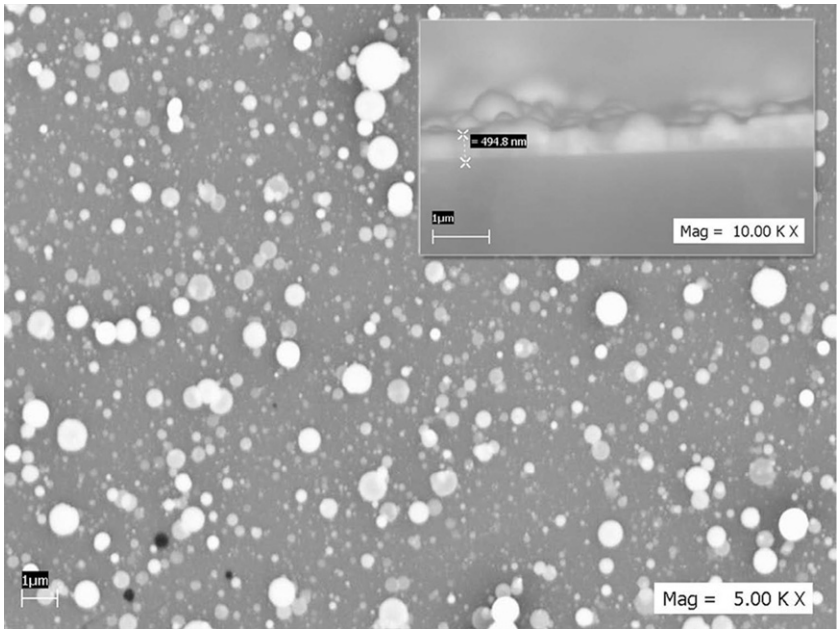

Fig. 3. Scanning electron microscopy image of $La_{0.66}Sr_{0.33}MnO_3$ surface morphology and profile (inset) showing the film thickness.

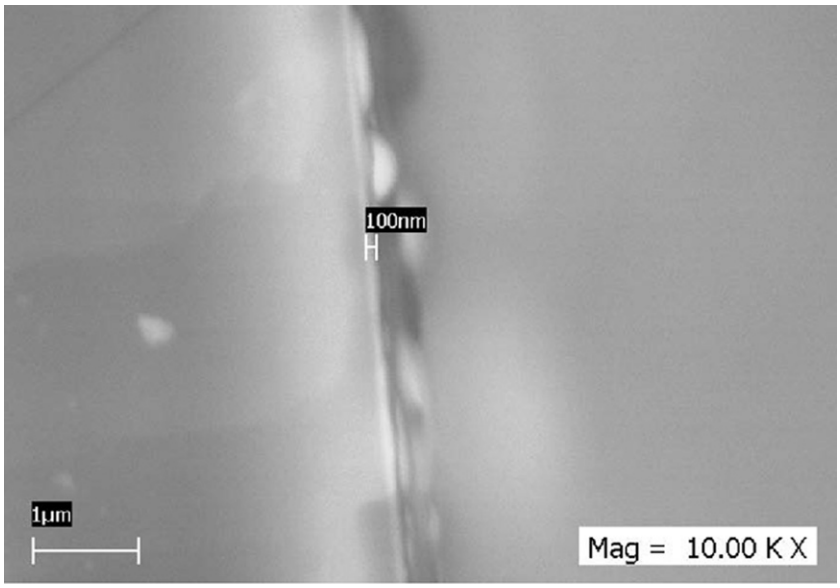

Fig. 4. Scanning electron microscopy image for a $La_{0.66}Sr_{0.33}MnO_3$ profile showing a film thickness of 100 nm.

first two compositions (15% and 33% of Sr) the overall absorption is very similar and much lower than for the 40% sample.

Additionally, the dielectric function for the three compositions showed similar main oscillators' energies around 4.7 eV while the other two oscillators changed slightly with the Sr concentration. Oscillator 2 increased largely from 1.593 eV for the 40% Sr sample to 3.011 eV for the 15% Sr sample. Complete detail of the complex dielectric function parameters are shown in Table 2 for each film.

4. Discussion

The composition, structure and optical characterization of the films indicated that they were polycrystalline, having some variations in their properties due to the increased divalent dopant in the compound. However, the morphology of the films was similar for each composition, showing a slight difference between roughness in samples having different thickness, mainly due to the fact that the laser fluence used to produce the films was sufficiently high to extract large portions of the target

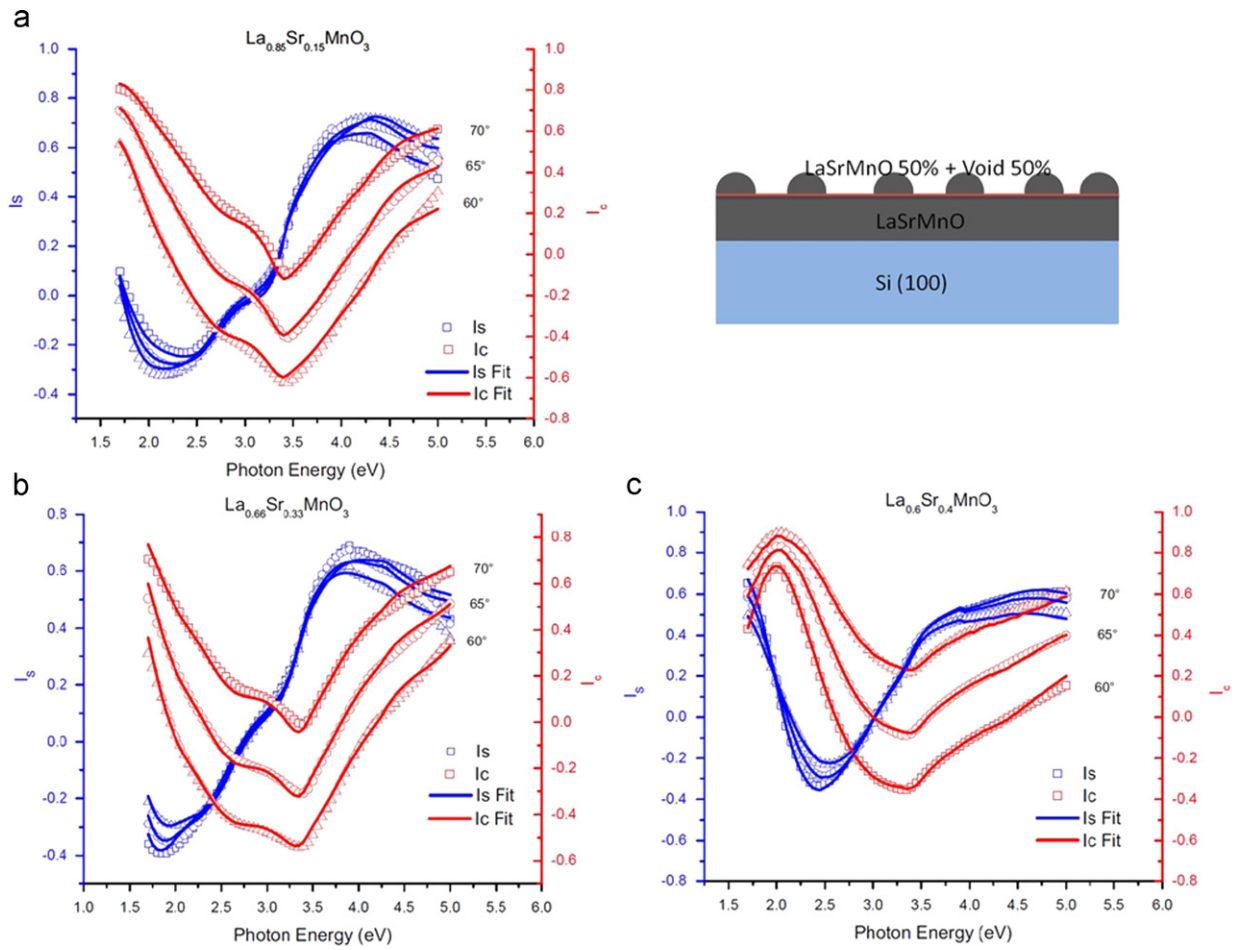

Fig. 5. Measured (dots) and fitted (lines) values of the ellipsometry data; *Is* and *Ic* for the three different acquisition angles, *Is* and *Ic* are correlated to the ellipsometry parameters as $Is = \sin 2\Psi \sin \Delta$ and $Ic = \sin 2\Psi \cos \Delta$. The three spectra were fitted simultaneously to obtain the film optical parameters, thickness and roughness of the layer (structural model showed in the inset). (a) 15% of strontium, (b) 33% of strontium, and (c) 40% of strontium.

Table 2
Complex dielectric function spectra parameters for $La_{1-x}Sr_xMnO_3$.

		Strontium percentage		
		15%	**33%**	**40%**
Thickness (nm)		94.1 ± 1.0	107.1 ± 0.7	94.7 ± 1.7
Thickness (roughness layer) (nm)		15.6 ± 0.5	10.8 ± 0.4	15.4 ± 0.9
Dielectric constant at infinite frequency	ε_∞	3.37 ± 0.02	3.26 ± 0.02	2.03 ± 0.04
Dielectric constant at static frequency	ε_s	3.92 ± 0.04	3.80 ± 0.04	3.57 ± 0.05
Oscillator energy (eV)	ω_t	4.80 ± 0.03	4.64 ± 0.02	4.69 ± 0.07
First oscillator's damping parameter	Γ_0	2.17 ± 0.12	2.15 ± 0.11	3.28 ± 0.14
Second oscillator's amplitude	f_1	0.31 ± 0.06	0.18 ± 0.04	0.02 ± 0.01
Second oscillator energy (eV)	ω_{01}	2.30 ± 0.06	2.17 ± 0.04	2.15 ± 0.05
Second oscillator's damping parameter	γ_1	1.28 ± 0.18	0.86 ± 0.11	0.53 ± 0.22
Third oscillator's amplitude	f_2	0.17 ± 0.04	0.27 ± 0.04	0.21 ± 0.08
Third oscillator energy (eV)	ω_{02}	3.01 ± 0.02	2.91 ± 0.02	1.59 ± 0.05
Third oscillator's damping parameter	γ_2	0.92 ± 0.11	1.12 ± 0.12	0.77 ± 0.23

(droplets) which enlarge the roughness of films, since increasing the deposition time the droplets' density on the surface will also increase.

On the other hand, it is well known that manganese ions determine the magnetic properties of the manganites, since they contribute with five degenerated levels into the 3d atomic level, split into 3 sublevels, t_{2g} and 2 e_g due to the crystal field of the oxygen ions [11]. Hence, transitions between the sublevels of Mn^{+3} and Mn^{+4} d levels are expected. Consequently, the electronic

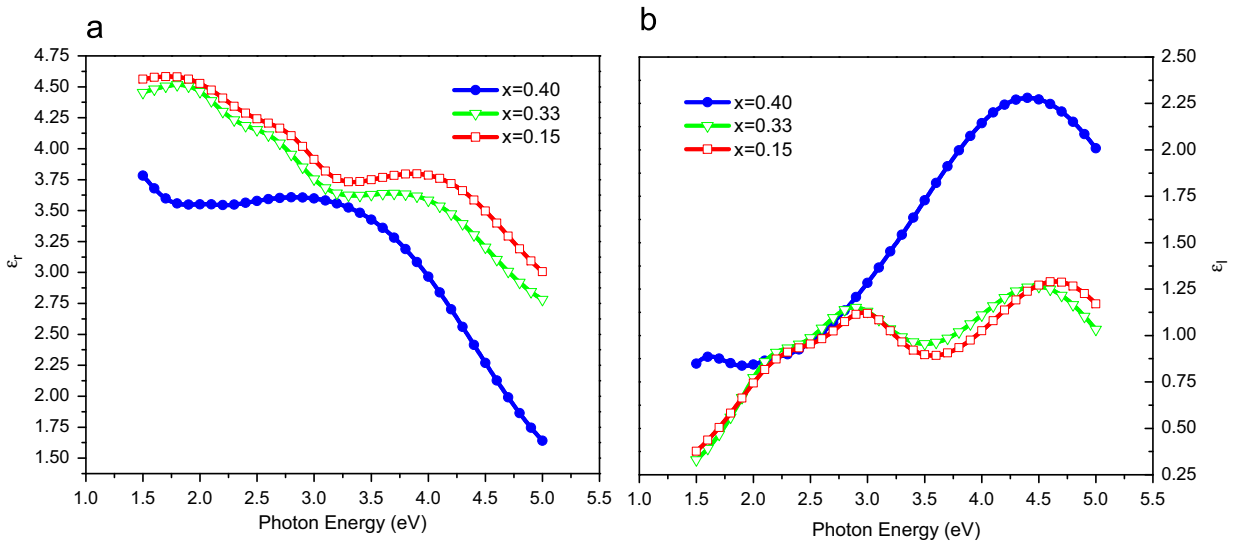

Fig. 6. Dielectric function of $L_{1-x}Sr_xMnO_3$ for $x=15\%$, 33% and 40% of strontium; (a) real and (b) imaginary part.

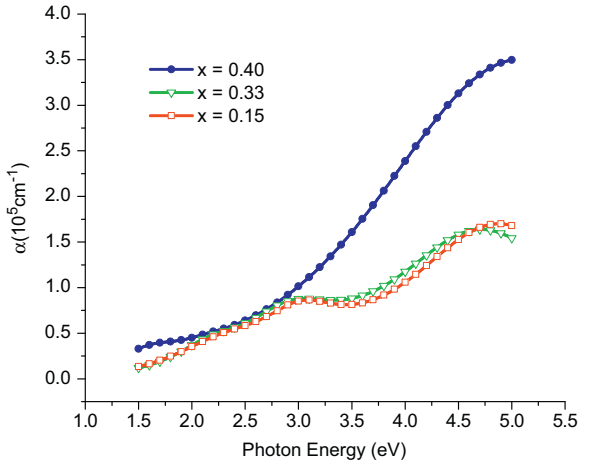

Fig. 7. Absorption coefficient for $La_{1-x}Sr_xMnO_3$ at room temperature. (□) $x=0.15$, (▽) $x=0.33$ and (●) $x=0.40$.

transition obtained by the ellipsometric results at 2.2 and 4.7 eV could be identified as for non-doped manganite $LaMnO_3$ as follows [12]: the transition at 2.2 eV takes place between d–d levels $e_g \rightarrow t_{2g}$ for high-spin Mn^{3+} ions, while the 4.7 eV transition is defined as a strong charge-transfer transition. Additionally, Noh et al. [13] have mentioned that the transition at 4.7 eV can be ascribed to charge transfer transition between the O 2p and the Mn d levels (t_{2g}), while transitions around 2–2.5 should come from e_g^1 to e_g^2 transition, thereby disagreeing with Arima and Tokum [14], who claim that this transition is due to O 2p to e_g levels. From our results, we suggest that the oscillator around 2.2 eV is due to the electronic transition at e_g^1 to e_g^2 levels since the energy of this transition is maintained for the three compositions (see Table 2).

Some other researchers have theoretically defined a third transition within the range studied in this report at 3.5 eV [3], which presumably originates from the interband transitions between the Hund's rule split bands. However, this transition was found at lower energies than that mentioned above, around 3.0 eV and only for the lower compositions, possibly due to the fact that the sample with 40% of strontium has more unpaired electrons, and therefore, the splitting of the energy levels is much smaller.

Moreover, the only composition showing the 1.6 eV peak, supporting the theory depicted by Kaplan and Mahanti [8] is the film with 40% of strontium. This peak has been assigned to interatomic transitions which depends on the symmetry of the Mn–O octahedron and therefore, altered by changing the content of dopant in the manganites which could indicate that it is moved to lower energies for the others compositions. However, this peak is extremely near to the limit of the range which prevents its accurate determination.

Systematically doping $LaMnO_3$ with strontium led to obtaining a clear understanding of the low energy optical transition. Fig. 7 shows the evolution of the $LaSrMnO_3$ absorption coefficient at room temperature for different Sr%. The increase in the absorption coefficient for the 40% of strontium sample reveals a change in the electronic states of the films. The Sr content plays a significant role on the electronic transition from isolator to metallic behavior in manganites, as it is described by Gor'kov and Kresin [1]. Increasing the strontium percentage leads to a rise in the density of states in the material. Therefore, the sample with 40% of strontium is expected to have higher absorption coefficient since it presents a more metallic behavior while the samples with lower content of strontium will present lower absorption coefficient.

5. Conclusions

$La_{1-x}Sr_xMnO_3$ was successfully synthesized by solid state reaction and grown on Si (1 0 0) substrates. Optical studies gave valuable information regarding the electronic structure of materials and about charge carriers. Ellipsometry studies clearly showed electronic transitions at 2.2 and 4.7 eV for all

the coatings related to Mn $e_g^1 \rightarrow e_g^2$ and O 2p→Mn t_{2g} levels transitions, respectively. It was demonstrated that a slight change in the composition and a small variation of the dopant in the manganite $LaSrMnO_3$ lead to different behavior for the structural as well as for the electrical transitions.

Acknowledgments

The work was financed by the Universidad Nacional de Colombia, Research Grant in 2006.

References

[1] Lev P. Gor'kov, Vladimir Z. Kresin, Physics Reports 400 (2004) 149–208.
[2] E.L. Nagaev, Physics Letters A 269 (2000) 357–362.
[3] E. Dagotto, T. Hotta, A. Moveo, Physics Reports 344 (2001) 1–153.
[4] S.Y. Yang, W.L. Kuang, Y. Liou, W.S. Tse, S.F. Lee, Y.D. Yao, Journal of Magnetism and Magnetic Materials 268 (2004) 326–331.
[5] M. Sirena, L. Steren, J. Guimpel, Thin Solid Films 373 (2000) 102–106.
[6] M.C. Terzzoli, D. Rubi, S. Duhalde, M. Villafuerte, M. Sierra, L. Steren, Applied Surface Science 186 (2002) 458–462.
[7] Y. Moritomo, A. Machida, K. Matsuda, M. Ichida, A. Nakamura, Physical Review B 56 (1997) 5088.
[8] T.A. Kaplan, S.D. Mahanti, Physics of Manganites 184 (1999).
[9] S. Calderón V, L. Escobar-Alarcón, Enrique Camps, S. Muhl, M. Rivera, I. Bentacourt, et al., Microelectronics Journal 39 (2008) 1281–1283.
[10] B Drevillon, Progress in Crystal Growth and Characterization of Materials 27 (1993) 1.
[11] R. Rauer, G. Neuber, J. Kunze, J. Backstrom, M. Rubhausen, T. Walter, et al., Journal of Magnetism and Magnetic Materials 290–291 (2005) 948–951.
[12] E. Gan'shina, N. Loshkareva, Yu. Sukhorukov, E. Mostovshchikova, A. Vinogradov, L. Nomerovannaya, Journal of Magnetism and Magnetic Materials 300 (2006) 62–66.
[13] T.W. Noh, J.H. Jung, K.H. Kim, Physics of Manganites (2002) 177–196.
[14] T. Arima, Y. Tokum, Journal of the Physical Society of Japan 64 (1995) 2488.